Towards a supercooled water guideline

V. Holten, M. A. Anisimov, and J. V. Sengers
Institute for Physical Science and Technology and
Department of Chemical and Biomolecular Engineering,
University of Maryland, College Park, Maryland 20742, U.S.A.

Technical Report
prepared for the
International Association for the Properties of Water and Steam

September 2012

Contents

Abstract

A status report is presented concerning the currently available experimental information for the thermodynamic properties of supercooled water and the possibility of modeling these thermodynamic properties on a theoretical basis. Part of the interest into the thermodynamic behavior of supercooled water is caused by an anomalous temperature dependence of the heat capacity, the compressibility and the thermal expansivity. We show that by assuming the existence of a liquid–liquid critical point in the unstable region at a very low temperature, we can give an accurate account of the experimental thermodynamic-property data in the experimentally accessible supercooled region. The resulting preliminary correlation is valid down to the homogeneous ice nucleation temperature and up to 400 MPa, the highest pressure where experimental data exist. The location in the phase diagram where the correlation for the supercooled region can be smoothly connected to the IAPWS-95 formulation is also shown.

1 Introduction

The peculiar thermodynamic behavior of supercooled water is currently receiving considerable attention. Upon supercooling, water exhibits an anomalous increase of its isobaric heat capacity and its isothermal compressibility, and an anomalous decrease of its expansivity coefficient.[1] One thermodynamically consistent explanation, originally proposed by Poole et al.,[2] is based on the presumed existence of a liquid–liquid critical point (LLCP) in water deep in the supercooled region. The hypothesis of the existence of a critical point in metastable water has been considered by many authors as recently reviewed by Bertrand and Anisimov.[3]

Several authors have made attempts to develop a thermodynamic model for the thermodynamic properties of supercooled water based on the LLCP scenario.[3–6] A model based on the existence of the LLCP is a good starting point for an empirical correlation for the properties of supercooled water, since the anomalous behavior is already built-in. A previous report[7] and article[8] described how a model based on critical scaling theory could be used to describe the data on supercooled water. Since then, we have obtained results that allow improvement of the correlation. Holten et al.[9] showed that a mean-field equation of state can describe the properties of supercooled water with the same quality as scaling theory. This result enables the use of a computationally simpler mean-field model as the basis of the correlation. Recently, Holten et al.[10] developed an explicit equation of state that incorporates the LLCP. This equation allows the use of a liquid–liquid transition (LLT) that is curved in the phase diagram, while the previous models had a straight-line LLT. In this report, a correlation based on the equation of state of Ref. 10 is presented that represents almost all the thermodynamic data on cold super and supercooled water.

2 Experimental data

Experimental data on the following properties were selected as input for the new correlation: density, thermal expansivity, isothermal compressibility, isobaric heat capacity, and speed of sound. Experimental data on the density, thermal expansivity and compressibility of cold and supercooled water have been reviewed in Ref. 8, and their location in the phase diagram is shown in Fig. 1. The location of the available speed-of-sound data, including some data near the melting curve at high pressures that have recently become available,[11,12] is shown in Fig. 2. These speed-of-sound data were not included in the fits of the models of Refs. 8 and 10.

Because the experimental data in Fig. 1 in the supercooled region are limited to pressures of 400 MPa and lower, the pressure range of validity of the present correlation is 0 MPa to 400 MPa. In temperature, the range of validity is bounded by the homogeneous ice nucleation curve, for which a correlation is presented in Appendix A. At higher temperatures, it is desirable that the present correlation agrees with the IAPWS-95 formulation. Based on the comparison of IAPWS-95 with experimental expansivity data that was made in Ref. 8, a region in the phase diagram

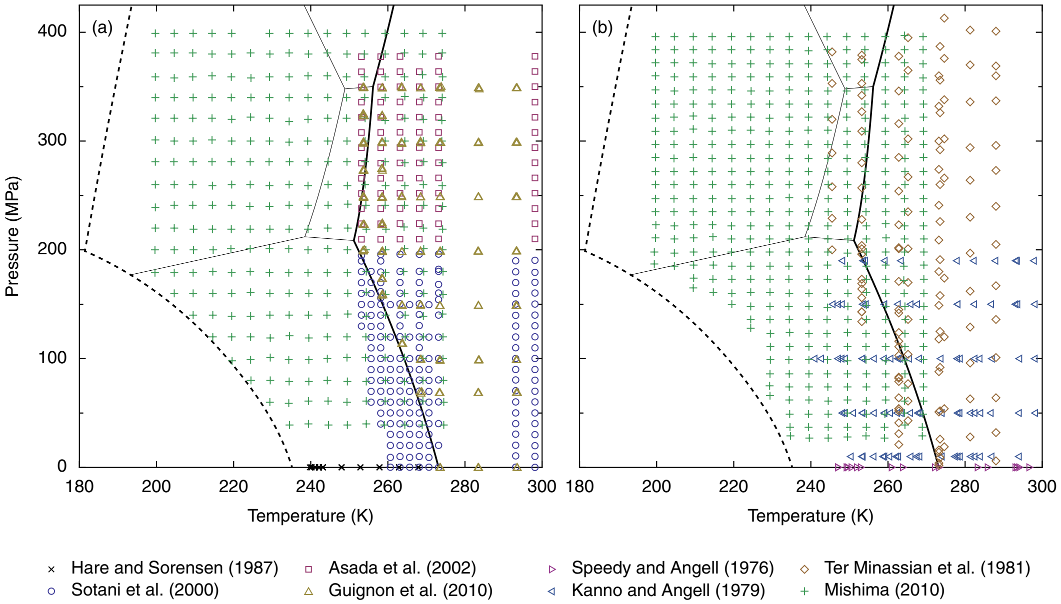

Figure 1: (a) Location of the experimental H_2O density data[13–17]. The thick solid curve is the solid–liquid phase boundary,[18] the dashed curve is the homogeneous ice nucleation limit (Appendix A), and the thin solid curves are the solid–solid phase boundaries.[19,20] (b) Location of the experimental H_2O density-derivative data. Ter Minassian et al.[21] have measured the expansivity coefficient, other authors[16,22,23] have measured the isothermal compressibility.

was estimated where values from IAPWS-95 could be used as input data to fit the new correlation to. Figure 3 shows the region where a representative selection of the experimental data was used for fitting the correlation, as well as the region where only values from IAPWS were used as input for the fit, up to a temperature of 324 K. The total number of data points used for the fit is 385, of which 198 are values from the IAPWS-95 formulation.

3 Equation of state

The equation of state that forms the basis of the current correlation is described in Ref. 10. It is a so-called two-state model, which assumes that liquid water is a mixture of a low-density and a high-density structure. We introduce the dimensionless quantities

$$\begin{aligned} \hat{T} &= \frac{T}{T_\mathrm{c}}, \quad \hat{G} = \frac{G}{RT_\mathrm{c}}, \quad \hat{V} = \frac{V}{V_\mathrm{c}}, \\ \tau &= \frac{T - T_\mathrm{c}}{T_\mathrm{c}}, \quad \pi = \frac{(P - P_\mathrm{c})V_\mathrm{c}}{RT_\mathrm{c}}, \end{aligned} \tag{1}$$

where T is the temperature, G is the molar Gibbs energy, R is the gas constant, P is the pressure and V is the molar volume. Values at the critical point are denoted

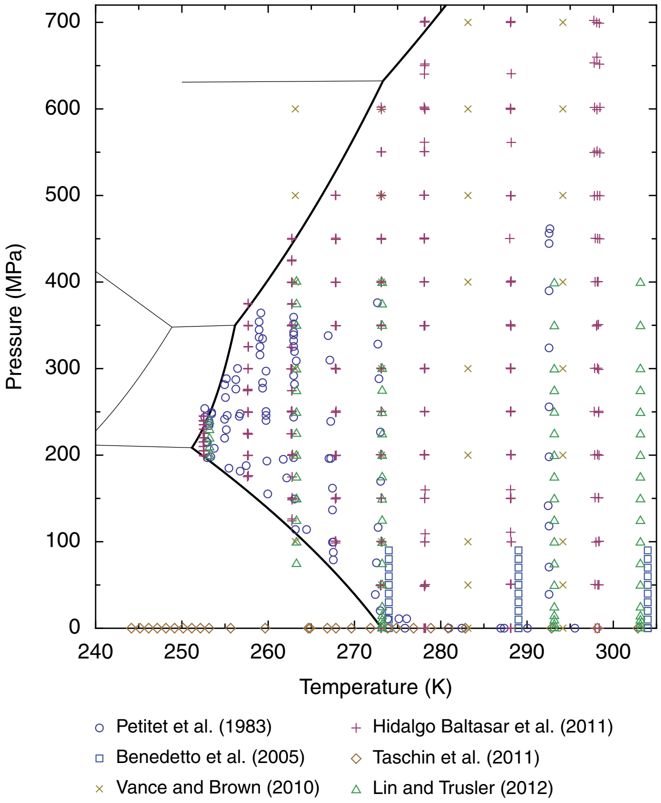

Figure 2: Location of experimental data on the speed of sound.[11,12,24–27] The thick curve is the solid–liquid phase boundary,[18] and the thin curves are the solid–solid phase boundaries.[19,20]

with a subscript c. The equation of state is

$$\frac{\hat{G}}{\hat{T}} = \frac{\hat{G}^{\mathrm{A}}}{\hat{T}} + xL + x\ln x + (1-x)\ln(1-x) + \omega x(1-x), \tag{2}$$

where x is the fraction of the low-density structure. The field L is given by

$$L(\tau,\pi) = \lambda(\tau + a\pi + b\tau\pi), \tag{3}$$

and the interaction parameter ω by

$$\omega(\pi) = 2 + \omega_0\pi. \tag{4}$$

$\hat{G}^{\mathrm{A}}$ is the the noncritical part of the Gibbs energy, the Gibbs energy of pure A, and is represented by

$$\hat{G}^{\mathrm{A}}(\tau,\pi) = \sum_{i=1}^{n} c_i \tau^{a_i}\pi^{b_i} + \sum_{i=n+1}^{m} c_i \tau^{a_i}\pi^{b_i}\exp(-\pi), \tag{5}$$

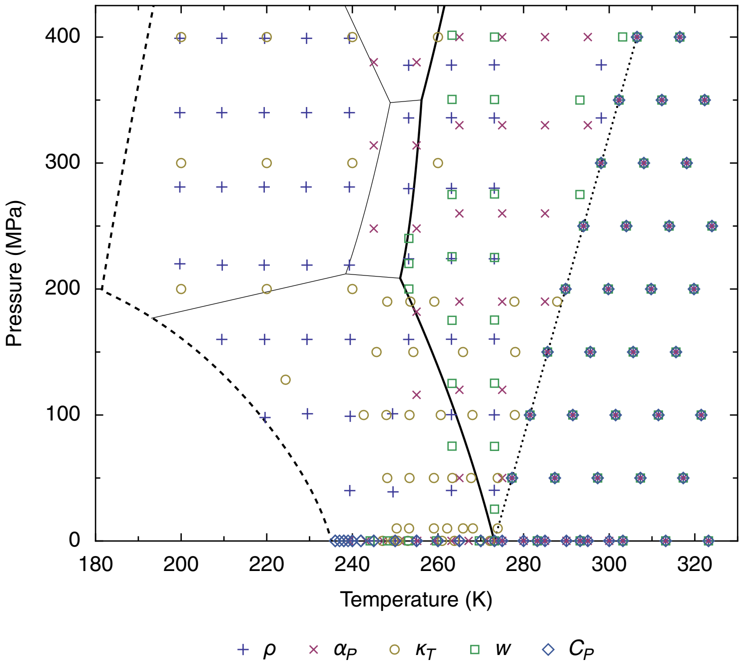

Figure 3: Location of the experimental data on density ρ, thermal expansivity α_P, isothermal compressibility κ_T, speed of sound w, and isobaric heat capacity C_P that were selected as input for the fit. To the right of the dotted line, the source of the data is the IAPWS-95 formulation.

where a_i, b_i, and c_i are adjustable coefficients.

At a certain pressure and temperature, the equilibrium fraction x_e is found from the condition

$$\left(\frac{\partial G}{\partial x}\right)_{T,P} = 0 \quad \text{at} \quad x = x_\mathrm{e}, \tag{6}$$

which yields

$$L + \ln\frac{x_\mathrm{e}}{1 - x_\mathrm{e}} + \omega(1 - 2x_\mathrm{e}) = 0. \tag{7}$$

This equation must be solved numerically for the fraction x_e.

It is convenient to express the thermodynamic properties in terms of the scaling fields and scaling susceptibilities. The scaling fields ϕ_1 and ϕ_2 are given by

$$\phi_1 = 2x_\mathrm{e} - 1, \qquad \phi_2 = -\tfrac{1}{2}\omega_0\phi_1^2. \tag{8}$$

The scaling susceptibility χ_1 is given by

$$\chi_1 = \left(\frac{2}{1 - \phi_1^2} - \omega\right)^{-1}. \tag{9}$$

The dimensionless volume can then be written as

$$\hat{V} = \frac{\hat{T}}{2}\left[\phi_2 + \frac{\omega_0}{2} + L_\pi(\phi_1 + 1)\right] + \hat{G}^\mathrm{A}_\pi, \tag{10}$$

with subscripts τ and π indicating partial derivatives, i.e.,

$$L_\tau = (\partial L/\partial\tau)_\pi = \lambda(1 + b\pi), \tag{11}$$

$$L_\pi = (\partial L/\partial\pi)_\tau = \lambda(a + b\tau). \tag{12}$$

The dimensionless response functions, namely isothermal compressibility $\hat{\kappa}_T$, expansion coefficient $\hat{\alpha}_P$, and isobaric heat capacity $\hat{C}_P$, are given by

$$\hat{\kappa}_T = \frac{1}{\hat{V}}\left[\frac{\hat{T}}{2}\chi_1(L_\pi - \omega_0\phi_1)^2 - \hat{G}^{\mathrm{A}}_{\pi\pi}\right], \tag{13}$$

$$\begin{aligned}\hat{\alpha}_P = \frac{1}{\hat{V}}\bigg\{&\frac{L_{\tau\pi}}{2}\hat{T}(\phi_1 + 1) + \frac{1}{2}\left[\phi_2 + \frac{\omega_0}{2} + L_\pi(\phi_1 + 1)\right] \\ &- \frac{\hat{T}L_\tau}{2}\chi_1(L_\pi - \omega_0\phi_1) + \hat{G}^{\mathrm{A}}_{\tau\pi}\bigg\},\end{aligned} \tag{14}$$

$$\hat{C}_P = -L_\tau\hat{T}(\phi_1 + 1) + \tfrac{1}{2}L_\tau^2\hat{T}^2\chi_1 - \hat{T}\hat{G}^{\mathrm{A}}_{\tau\tau}. \tag{15}$$

These dimensionless quantities are related to the quantities with dimensions according to

$$\kappa_T = \frac{\hat{\kappa}_T}{\rho_{\mathrm{c}}RT_{\mathrm{c}}}, \qquad \alpha_P = \frac{\hat{\alpha}_P}{T_{\mathrm{c}}}, \qquad C_P = R\hat{C}_P, \tag{16}$$

with the molar density $\rho = 1/V$. The molar isochoric heat capacity C_V is found from the thermodynamic relation

$$C_V = C_P - \frac{T\alpha_P^2}{\rho\kappa_T}, \tag{17}$$

and the speed of sound w from

$$w = \left(\tilde{\rho}\kappa_T\frac{C_V}{C_P}\right)^{-1/2} = \left(\tilde{\rho}\kappa_T - \frac{T\alpha_P^2}{\tilde{C}_P}\right)^{-1/2}, \tag{18}$$

where $\tilde{\rho} = M\rho$ and $\tilde{C}_P = C_P/M$ are the specific (mass-based) density and heat capacity, with M the molar mass. Numerical values of all parameters are listed in Appendix B.

Equation (2) is a mean-field equation of state that implies classical critical exponents. As shown in Refs. 8 and 9, a mean-field equation describes the experimental data equally well as a nonanalytic equation based on critical scaling theory. The reason that a mean-field approximation can be used is that the region asymptotically close to the critical point, where scaling theory would be necessary, is not experimentally accessible. Moreover, a mean-field equation of state is more convenient for computational use than one incorporating scaling theory.

4 Comparison with experimental data

The density is shown as a function of temperature for several isobars in Fig. 4. The density data of Mishima[16] show systematic differences with the densities reported by Asada et al.[15] and IAPWS-95. To prevent this difference from affecting the current correlation, we have fitted the equation to a version of Mishima's data that was adjusted for this systematic difference, as described in Ref. 8. The adjustment is at most 0.35% in density, which is within the experimental uncertainty. The figures in this report show the original data of Mishima. The density deviations of the current correlation at atmospheric pressure are shown in Fig. 5, and the deviations for several isotherms are shown in Fig. 6. It is seen that the five density data sets agree with each other within the experimental uncertainty, and that the current correlation represents almost all of the data within their uncertainty.

The compressibility and expansivity are shown as a function of temperature in Fig. 7 and Fig. 8. The new correlation agrees well with the data, except for a few expansivity data points below 250 K at atmospheric pressure. However, these points do not represent direct measurements of the expansivity, but were derived from smoothed density values.[13]

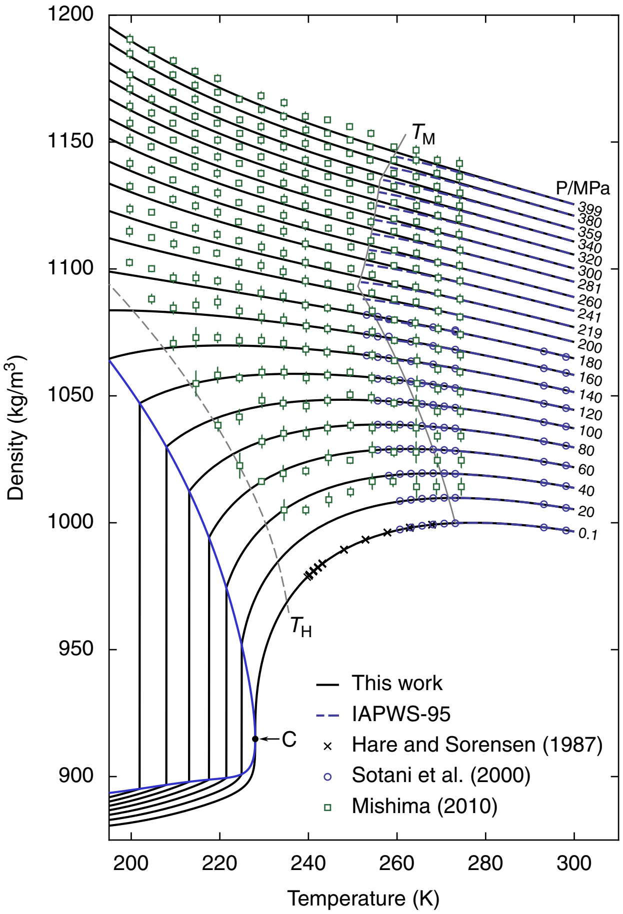

Figure 4: Density as a function of temperature and pressure. Black curves are calculated from the current correlation. Symbols represent experimental data.[13,14,16] T_M indicates the melting temperature and T_H indicates the homogeneous nucleation temperature. The blue curve is the liquid–liquid equilibrium curve, with the critical point C. Values from IAPWS-95 are plotted (dashed) for comparison in the range where it is valid.

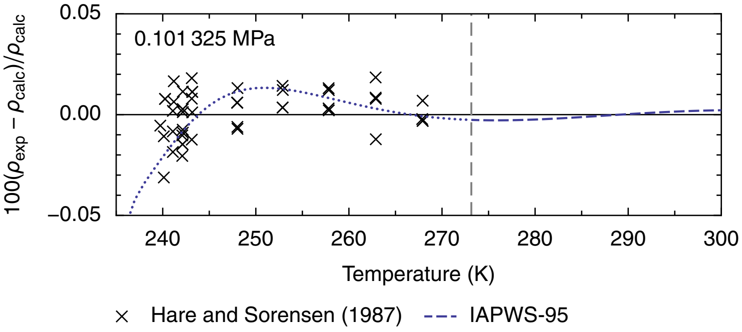

Figure 5: Percentage deviations between experimental density data[13] at atmospheric pressure and values calculated from the current correlation. Values calculated from IAPWS-95 are plotted for comparison; dashed in the stable-liquid region and dotted in the metastable region. The vertical dashed line indicates the melting temperature.

The heat capacity at constant pressure C_P and at constant volume C_V are shown in Fig. 9. The two data sets for C_P that extend down to the lowest temperature of 236 K, those of Angell et al.[28] and Archer and Carter[29], do not agree with each other below about 255 K. Both data sets were included in the fit, and the correlation gives values in between them. There are no measurements for C_V of supercooled water, so the C_V curve in Fig. 9 represents only a prediction.

Deviations between experimental data on the speed of sound and the current correlation are plotted in Fig. 10 and Fig. 11. Most of the data sets from different authors agree with each other, but the data of Hidalgo Baltasar et al.[11] deviate from the other data below 280 K and above 250 MPa. The relative deviations reach at most 0.8%, which is larger than the experimental uncertainty of 0.2% to 0.3%. The current fit is based on the data of Lin and Trusler[12] and Taschin.[27] The data of Lin and Trusler,[12] with a specified uncertainty of 0.03% to 0.04%, are not reproduced to within that accuracy but within about 0.1%. However, the empirical correlation that Lin and Trusler[12] fitted to their own data also deviates from their data by up to 0.15%.

5 Connecting to IAPWS-95

If the properties of water are to be represented in both the supercooled and the stable range, the new correlation should smoothly connect to the IAPWS-95 formulation at a certain boundary in the P–T diagram. A natural choice for this boundary is the melting curve, which is the boundary of the range of validity of IAPWS-95. As Fig. 12 illustrates, connecting at the melting curve will lead to jumps of more than 10% in the heat capacity and about 50% in the thermal expansivity. If better agreement or a smoother connection is desired, the connection temperature has to be increased. Because the expansivity is the quantity that differs most between the current correlation and IAPWS-95, the connection temperature should be based on that quantity. Figure 8 shows arrows at possible connection temperatures for different pressures. The connection temperature increases with pressure, and the proposed connection boundary in the phase diagram is shown in Fig. 12. Up to about 70 MPa the connection can be made at the melting curve, while at 400 MPa the connection temperature is about 305 K.

6 Discussion

We have presented a preliminary correlation that represents almost all thermodynamic-property data on cold and supercooled water. There are a number of issues that can be considered. First, the current correlation can be slightly improved by including more or different terms in the noncritical part of the Gibbs energy $\hat{G}^{\mathrm{A}}$. This would result in a smaller average deviation from experimental data, and would increase the fraction of data points that are represented within the experimental uncertainty. Second, the limit of validity is currently 400 MPa, because there are no experimental data above that pressure. Because the suggested correlation was not constrained for pressures higher than 400 MPa, it cannot be reliably extrapolated. With the inclusion of suitable constraints, the extrapolation behavior to higher pressures could be improved. Another issue is the extrapolation below the homogeneous nucleation temperature. Extrapolation in this region is sensitive to the location of the LLCP, where the thermodynamic response functions diverge. Since the existence of the LLCP is uncertain, it is at present not possible to specify what the extrapolation behavior should be. However, the region below the homogeneous nucleation temperature is currently inaccessible to experiments.

Acknowledgments

The research of V. Holten has been supported by the International Association for the Properties of Water and Steam. In addition, research of V. Holten and M.A. Anisimov has been supported by the Division of Chemistry of the US National Science Foundation under Grant No. CHE-1012052.

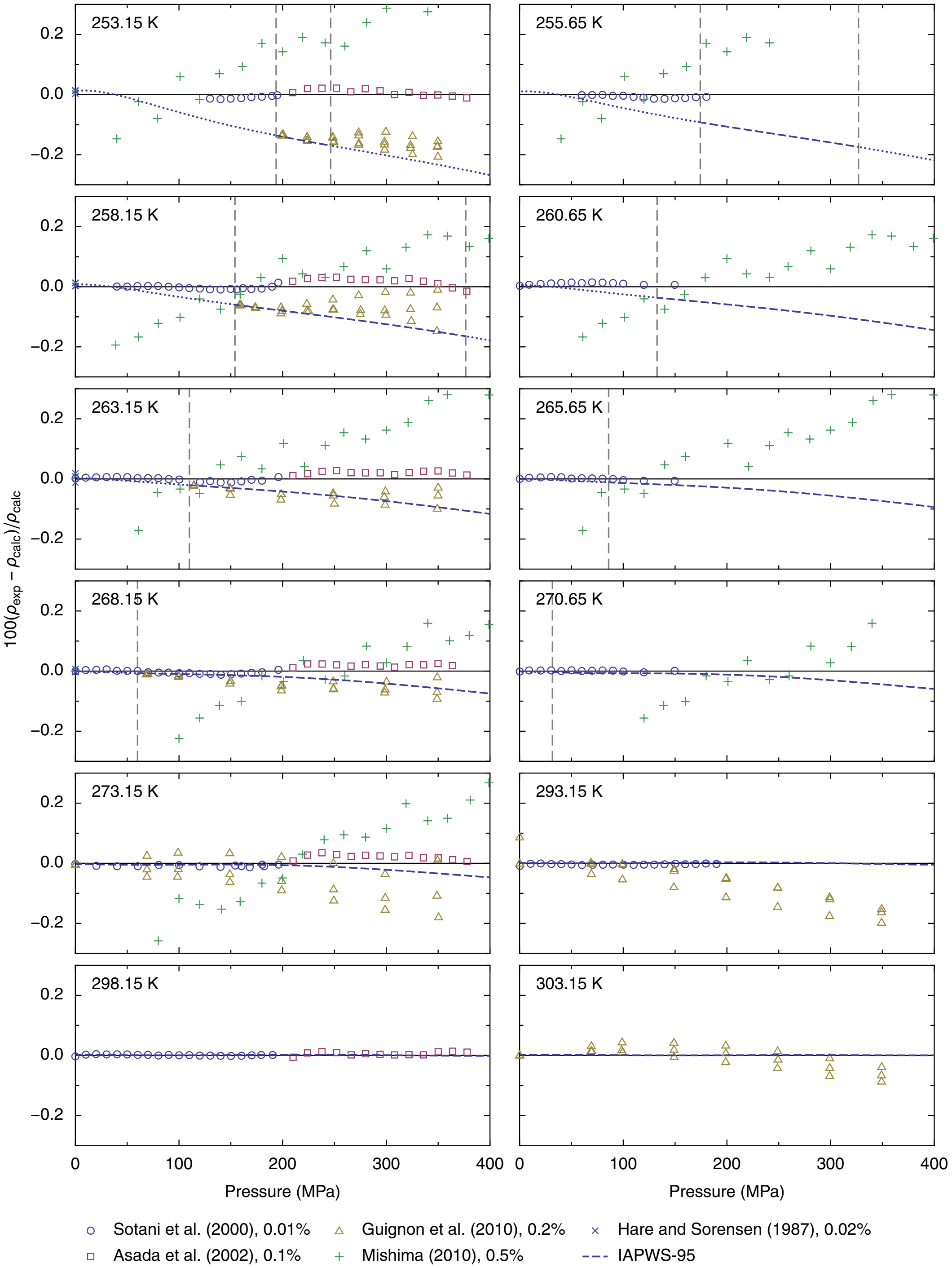

Figure 6: Percentage deviations between experimental density data and values calculated from the current correlation. The percentages listed in the legend are specified or estimated relative uncertainties of the data. Values calculated from IAPWS-95 are plotted for comparison; dashed in the stable-liquid region and dotted in the metastable region. The vertical dashed lines indicate the melting pressure.

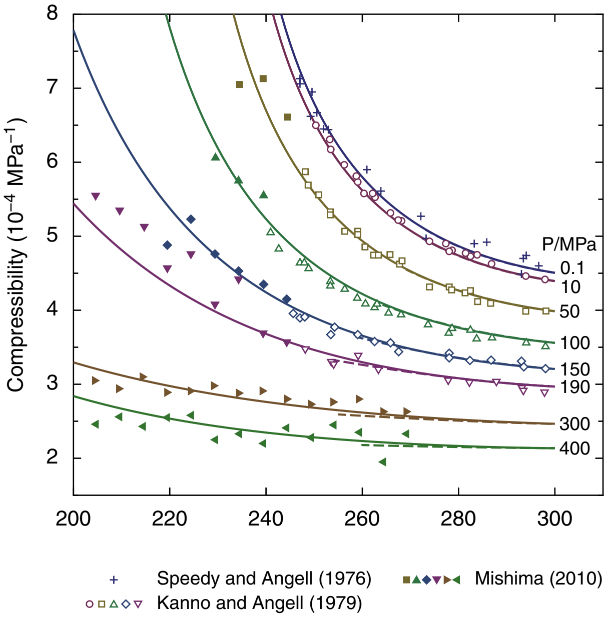

Figure 7: Isothermal compressibility calculated from the new correlation (solid curves). Symbols represent experimental data.[16,22,23] Solid and open symbols with the same shape correspond to the same pressure. Values from IAPWS-95 are plotted for comparison (dashed) in the range where it is valid.

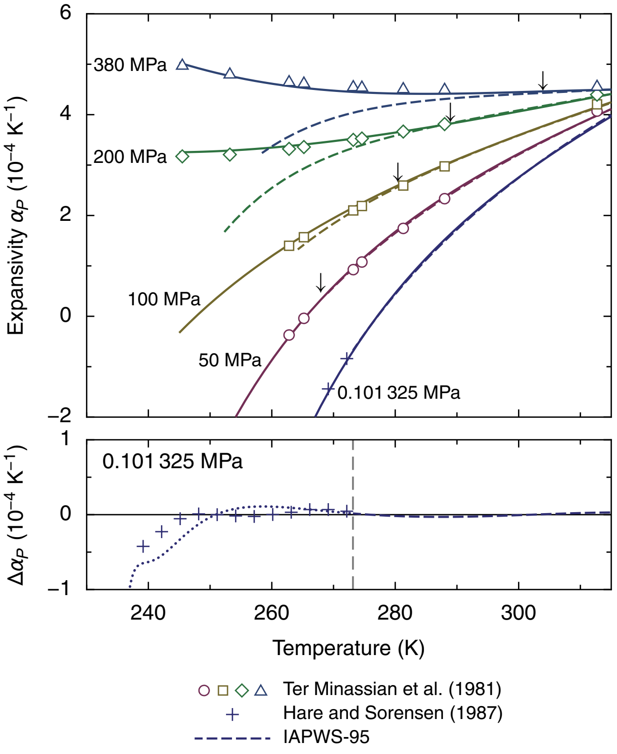

Figure 8: Thermal expansivity calculated from the new correlation (solid curves). Symbols represent experimental data of Ter Minassian et al.[21] and Hare and Sorensen.[13] Values from IAPWS-95 are plotted for comparison (dashed) in the range where it is valid. Arrows indicate temperatures where the new correlation can be smoothly connected to IAPWS-95. Bottom graph: deviation $\Delta\alpha_P = \alpha_{P,\text{exp}} - \alpha_{P,\text{calc}}$ between experimental data and the new correlation at atmospheric pressure. The vertical dashed line indicates the melting temperature.

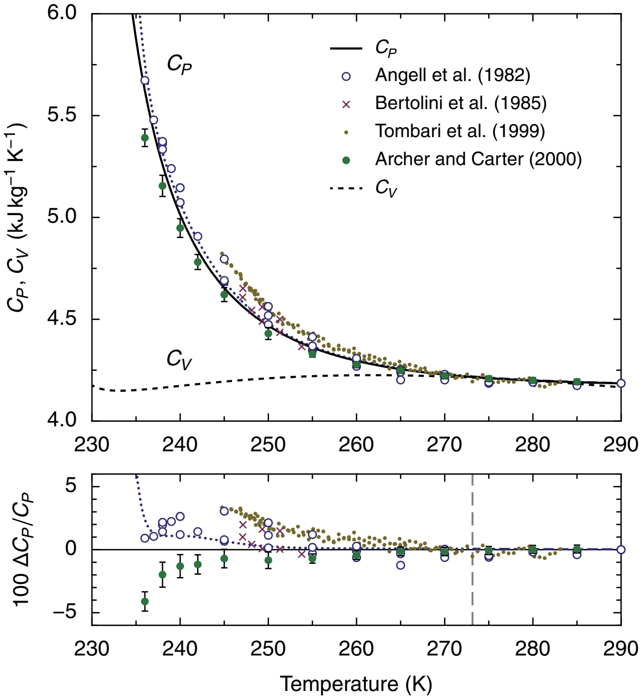

Figure 9: Heat capacity at atmospheric pressure calculated from the new correlation (solid curve: C_P, short-dashed curve: C_V). Symbols represent experimental data.[28–31] Values from IAPWS-95 are plotted for comparison in the range where it is valid; dashed in the stable-liquid region and dotted in the metastable region. Bottom graph: deviation $100\Delta C_P/C_P = 100(C_{P,\mathrm{exp}} - C_{P,\mathrm{calc}})/C_{P,\mathrm{calc}}$ between experimental data and the new correlation at atmospheric pressure. The vertical dashed line indicates the melting temperature.

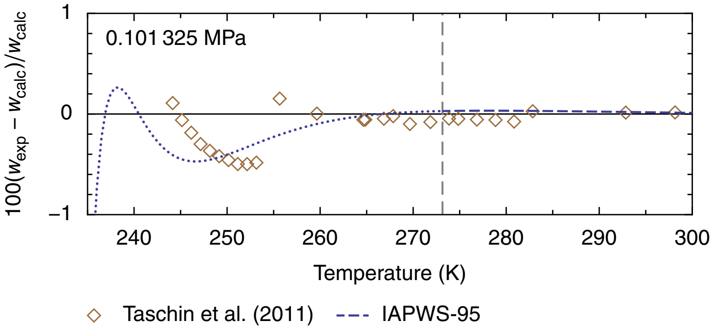

Figure 10: Percentage deviations between experimental speed-of-sound data[27] at atmospheric pressure and values calculated from the current correlation. For temperatures of 260 K and lower, the experimental data have uncertainties of 0.7%. Values calculated from IAPWS-95 are plotted for comparison; dashed in the stable-liquid region and dotted in the metastable region. The vertical dashed line indicates the melting temperature.

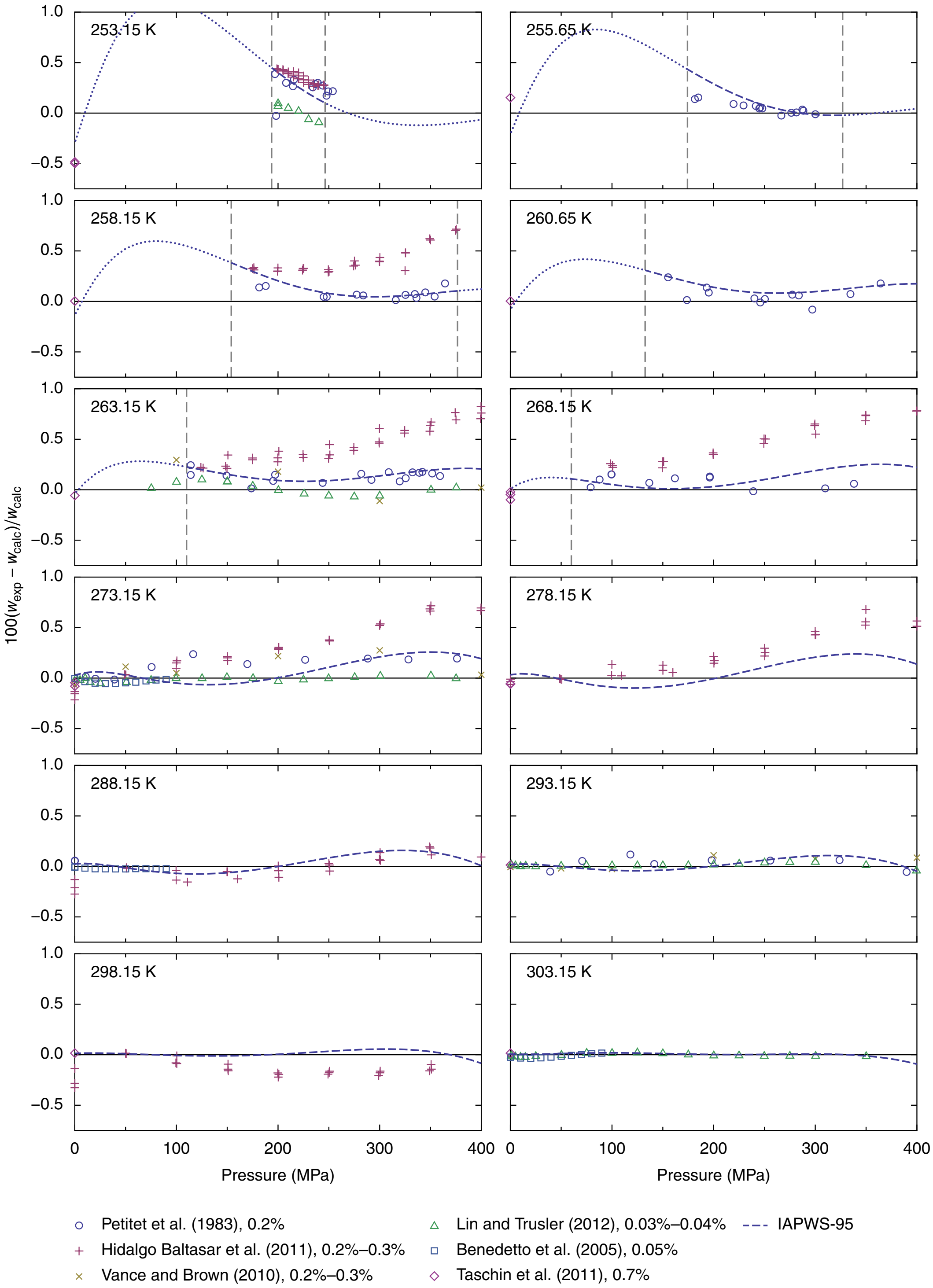

Figure 11: Percentage deviations between experimental data on the speed of sound and values calculated from the current correlation. The percentages listed in the legend are specified or estimated relative uncertainties of the data. Values calculated from IAPWS-95 are plotted for comparison; dashed in the stable-liquid region and dotted in the metastable region. The vertical dashed lines indicate the melting pressure.

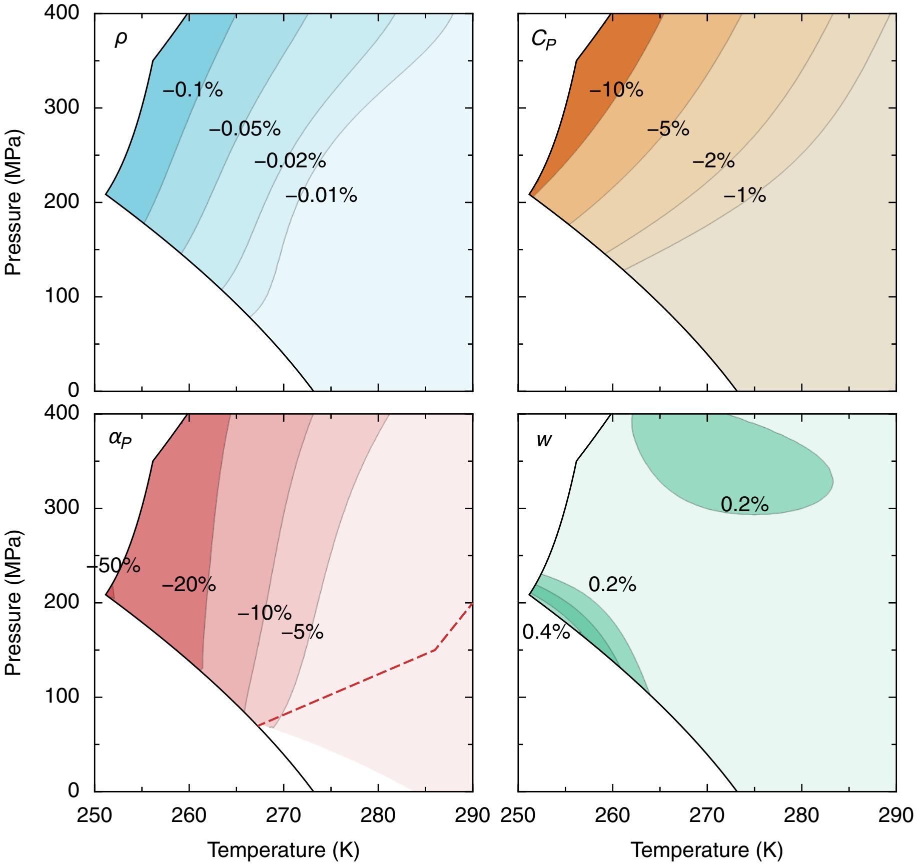

Figure 12: Percentage deviations between the IAPWS-95 formulation and the current correlation, for the density ρ, isobaric heat capacity C_P, thermal expansivity α_P, and speed of sound w. The dashed line is the proposed location where the new formulation should smoothly connect with IAPWS-95, based on the expansivity shown in Fig. 8.

Appendix A Homogenous ice nucleation temperature

Liquid water can be supercooled down to the homogenous ice nucleation temperature T_{H}, which is about 235 K at atmospheric pressure. At higher pressures, T_{H} is lower, with a minimum of 181 K at 200 MPa. The pressure dependence of T_{H} has been measured by Xans and Barnaud[32], Kanno et al.[33] and Kanno and Miyata[34] at pressures below 300 MPa; see Fig. 13. Mishima[35] has measured T_{H} at pressures from 500 MPa to 1500 MPa. At about 200 MPa, there is a break in the T_{H} curve as a result of nucleation of a different kind of ice above this pressure.[33,34] For pressures below the break point, the shape of the T_{H} curve can be described by an equation of the Simon type, which was also used by Wagner et al.[36] to describe the melting curves of water. A fit of such an equation to the data of Kanno et al.[33] and Kanno and Miyata[34] yields the pressure P_{H} on the homogeneous nucleation curve as a function of the temperature T,

$$P_{\mathrm{H}}/P_0 = 1 + 2282.7(1 - \theta^{6.243}) + 157.24(1 - \theta^{79.81}), \tag{19}$$

where $\theta = T/T_0$, $T_0 = 235.15$ K, and $P_0 = 0.1$ MPa. Above the break point, a third-order polynomial was fitted to the data, including Mishima's data up to 1500 MPa, yielding

$$T_{\mathrm{H}}/\mathrm{K} = 172.82 + 0.03718p + 3.403 \times 10^{-5} p^2 - 1.573 \times 10^{-8} p^3, \tag{20}$$

with $p = P/\mathrm{MPa}$. This polynomial is based on the assumption that the T_{H} curve is smooth at pressures above the break point. However, because of the lack of data

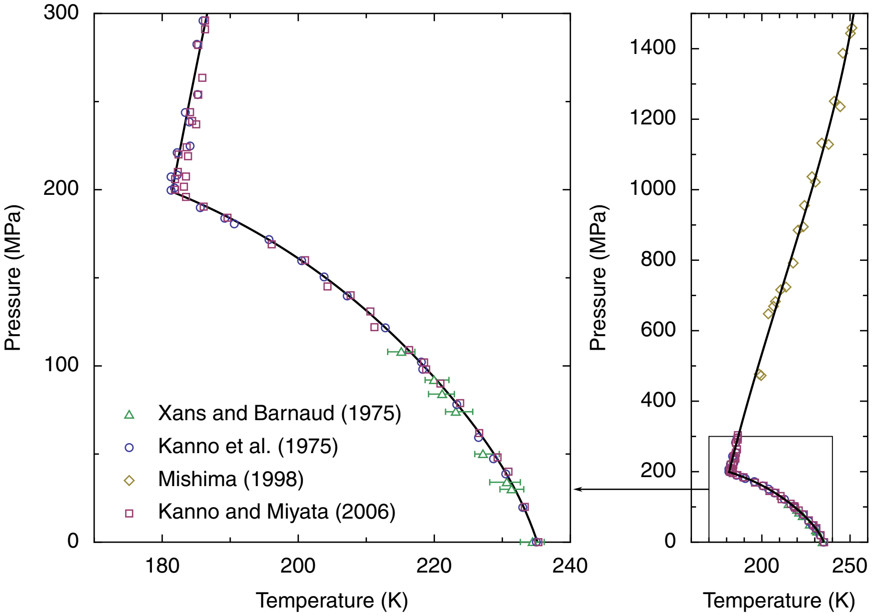

Figure 13: Temperature of homogenous ice nucleation. Symbols represent experimental data,[32–35] and the curve is given by Eqs. (19) and (20).

in the range of 300 MPa to 600 MPa, the existence of other break points in the curve cannot be excluded. Is must also be noted that unlike the melting curve, the homogenous nucleation curve is a kinetic limit and depends on the size and time scale of the experiment.

Appendix B Numerical values for the parameters

The numerical values for the parameters in the equation of state are listed below. The parameter c_1 is not independent; the constraint $\hat{V} = 1$ relates it to other parameters as $c_1 = 1 - \lambda a/2 - \omega_0/4 - c_{15}$.

Parameter	Value	Unit
T_c	228.0	K
P_c	0	MPa
ρ_c	914.844	kg m^{-3}
λ	2.77286	
ω_0	0.319082	
a	0.0612649	
b	−0.266775	
n	14	
m	20	
R	8.3144621	J mol^{-1} K^{-1}
M	18.015268	g/mol

i	c_i	a_i	b_i
1	$8.297\,264 \times 10^{-1}$	0	1
2	$-6.178\,979 \times 10^{-3}$	0	2
3	$1.785\,700 \times 10^{-1}$	1	1
4	$-3.579\,009 \times 10^{0}$	2	0
5	$-5.218\,701 \times 10^{-5}$	0	3
6	$-2.048\,750 \times 10^{-2}$	1	2
7	$-7.699\,798 \times 10^{-2}$	2	1
8	$1.940\,109 \times 10^{-3}$	1	3
9	$1.308\,921 \times 10^{-2}$	2	2
10	$9.912\,325 \times 10^{-1}$	4	0
11	$-2.993\,320 \times 10^{-3}$	2	3
12	$3.754\,090 \times 10^{-2}$	3	2
13	$-5.300\,774 \times 10^{-1}$	5	0
14	$-2.829\,167 \times 10^{-2}$	4	2
15	$5.563\,555 \times 10^{-3}$	0	1
16	$-6.567\,783 \times 10^{-2}$	1	0
17	$8.770\,874 \times 10^{-4}$	0	2
18	$-2.638\,605 \times 10^{-2}$	1	1
19	$-1.309\,306 \times 10^{-1}$	5	0
20	$8.365\,243 \times 10^{-3}$	3	3

References

1 P. G. Debenedetti, Supercooled and glassy water, *J. Phys.: Condens. Matter* **15**, R1669 (2003).

2 P. H. Poole, F. Sciortino, U. Essmann, and H. E. Stanley, Phase behaviour of metastable water, *Nature (London)* **360**, 324 (1992).

3 C. E. Bertrand and M. A. Anisimov, The peculiar thermodynamics of the second critical point in supercooled water, *J. Phys. Chem. B* **115**, 14099 (2011).

4 S.B. Kiselev, Physical limit of stability in supercooled liquids, *Int. J. Thermophys.* **22**, 1421 (2001).

5 S.B. Kiselev and J.F. Ely, Parametric crossover model and physical limit of stability in supercooled water, *J. Chem. Phys.* **116**, 5657 (2002).

6 D.A. Fuentevilla and M.A. Anisimov, Scaled equation of state for supercooled water near the liquid-liquid critical point, *Phys. Rev. Lett.* **97**, 195702 (2006), erratum *ibid.* **98**, 149904 (2007).

7 V. Holten, C.E. Bertrand, M.A. Anisimov, and J.V. Sengers, *Thermodynamic modeling of supercooled water*, Technical report prepared for the International Association for the Properties of Water and Steam (2011).

8 V. Holten, C.E. Bertrand, M.A. Anisimov, and J.V. Sengers, Thermodynamics of supercooled water, *J. Chem. Phys.* **136**, 094507 (2012).

9 V. Holten, J. Kalová, M.A. Anisimov, and J.V. Sengers, Thermodynamics of liquid–liquid criticality in supercooled water in a mean-field approximation, *Int. J. Thermophys.* **33**, 758 (2012).

10 V. Holten and M.A. Anisimov, Entropy-driven liquid–liquid separation in supercooled water, *Sci. Rep.* **2**, 713 (2012).

11 E. Hidalgo Baltasar, M. Taravillo, V.G. Baonza, P.D. Sanz, and B. Guignon, Speed of sound in liquid water from (253.15 to 348.15) K and pressures from (0.1 to 700) MPa, *J. Chem. Eng. Data* **56**, 4800 (2011).

12 C.-W. Lin and J.P.M. Trusler, The speed of sound and derived thermodynamic properties of pure water at temperatures between (253 and 473) K and at pressures up to 400 MPa, *J. Chem. Phys.* **136**, 094511 (2012).

13 D.E. Hare and C.M. Sorensen, The density of supercooled water. II. Bulk samples cooled to the homogeneous nucleation limit, *J. Chem. Phys.* **87**, 4840 (1987).

14 T. Sotani, J. Arabas, H. Kubota, and M. Kijima, Volumetric behaviour of water under high pressure at subzero temperature, *High Temp. High Pressures* **32**, 433 (2000).

15 S. Asada, T. Sotani, J. Arabas, H. Kubota, S. Matsuo, and Y. Tanaka, Density of water at subzero temperature under high pressure: measurements and correlation, *J. Phys.: Condens. Matter* **14**, 11447 (2002).

16 O. Mishima, Volume of supercooled water under pressure and the liquid-liquid critical point, *J. Chem. Phys.* **133**, 144503 (2010).

17 B. Guignon, C. Aparicio, and P.D. Sanz, Specific volume of liquid water from (253 to 323) K and pressures up to 350 MPa by volumetric measurements, *J. Chem. Eng. Data* **55**, 3338 (2010).

18 W. Wagner, T. Riethmann, R. Feistel, and A.H. Harvey, New equations for the sublimation pressure and melting pressure of H_2O ice Ih, *J. Phys. Chem. Ref. Data* **40**, 043103 (2011).

19 P.W. Bridgman, Water, in the liquid and five solid forms, under pressure, *Proc. Am. Acad. Arts Sci.* **47**, 441 (1912).

20 G.S. Kell and E. Whalley, Equilibrium line between ice I and III, *J. Chem. Phys.* **48**, 2359 (1968).

21 L. Ter Minassian, P. Pruzan, and A. Soulard, Thermodynamic properties of water under pressure up to 5 kbar and between 28 and 120°C. Estimations in the supercooled region down to −40 °C, *J. Chem. Phys.* **75**, 3064 (1981).

22 R.J. Speedy and C.A. Angell, Isothermal compressibility of supercooled water and evidence for a thermodynamic singularity at −45°C, *J. Chem. Phys.* **65**, 851 (1976).

23 H. Kanno and C.A. Angell, Water: Anomalous compressibilities to 1.9 kbar and correlation with supercooling limits, *J. Chem. Phys.* **70**, 4008 (1979).

24 J.P. Petitet, R. Tufeu, and B. Le Neindre, Determination of the thermodynamic properties of water from measurements of the speed of sound in the temperature range 251.15–293.15 K and the pressure range 0.1–350 MPa, *Int. J. Thermophys.* **4**, 35 (1983).

25 G. Benedetto, R.M. Gavioso, P.A. Giuliano Albo, S. Lago, D. Madonna Ripa, and R. Spagnolo, Speed of sound in pure water at temperatures between 274 and 394 K and at pressures up to 90 MPa, *Int. J. Thermophys.* **26**, 1667 (2005).

26 S. Vance and J.M. Brown, Sound velocities and thermodynamic properties of water to 700 MPa and −10 to 100 °C, *J. Acoust. Soc. Am.* **127**, 174 (2010).

27 A. Taschin, R. Cucini, P. Bartolini, and R. Torre, Does there exist an anomalous sound dispersion in supercooled water?, *Phil. Mag.* **91**, 1796 (2011).

28 C.A. Angell, M. Oguni, and W.J. Sichina, Heat capacity of water at extremes of supercooling and superheating, *J. Phys. Chem.* **86**, 998 (1982).

29 D.G. Archer and R.W. Carter, Thermodynamic properties of the NaCl + H_2O system. 4. Heat capacities of H_2O and NaCl(aq) in cold-stable and supercooled states, *J. Phys. Chem. B* **104**, 8563 (2000).

30 D. Bertolini, M. Cassettari, and G. Salvetti, Anomalies in the "latent heat" of solidification of supercooled water, *Chem. Phys. Lett.* **199**, 553 (1985).

31 E. Tombari, C. Ferrari, and G. Salvetti, Heat capacity anomaly in a large sample of supercooled water, *Chem. Phys. Lett.* **300**, 749 (1999).

32 P. Xans and G. Barnaud, A study as a function of pressure (P < 1,100 bars) of the spontaneous freezing of droplets of supercooled and deuterated water (volumes of a few mm^3 and of a few μ^3), *C. R. Acad. Sci. Paris* **280**, 25 (1975).

33 H. Kanno, R.J. Speedy, and C.A. Angell, Supercooling of water to −92 °C under pressure, *Science* **189**, 880 (1975).

34 H. Kanno and K. Miyata, The location of the second critical point of water, *Chem. Phys. Lett.* **422**, 507 (2006).

35 O. Mishima and H.E. Stanley, Decompression-induced melting of ice IV and the liquid–liquid transition in water, *Nature* **392**, 164 (1998).

36 W. Wagner, A. Saul, and A. Pruß, International equations for the pressure along the melting and along the sublimation curve of ordinary water substance, *J. Phys. Chem. Ref. Data* **23**, 515 (1994).